Available online at www.sciencedirect.com
ScienceDirect
Journal of the European Ceramic Society 27 (2007) 4797–4805
www.elsevier.com/locate/jeurceramsoc

Stability of ultra-high-temperature ZrB_2–SiC ceramics under simulated atmospheric re-entry conditions

Frédéric Monteverde [a,*], Raffaele Savino [b]

[a] *ISTEC, Institute of Science and Technology for Ceramics, National Research Council, Via Granarolo 64, 48018 Faenza, Italy*
[b] *DIAS, Dipartimento di Ingegneria Aerospaziale, University of Naples "Federico II", P.le V. Tecchio 80, 80125 Naples, Italy*

Received 12 October 2006; received in revised form 13 February 2007; accepted 18 February 2007
Available online 29 March 2007

Abstract

Microstructure modifications of an ultra-high temperature ZrB_2–SiC ceramic exposed to ground simulated atmospheric re-entry conditions were investigated and discussed. Fluid dynamic numerical calculations were carried out to correlate and explain the experimental results. The cross-sectioning of the ceramic models after exposure (examined by SEM) showed a compact scale of zirconia (20 μm thick) underlying an external silica thin coating. A partially SiC-depleted region, a few microns thick, underneath the zirconia sub-scale was also seen. The post-test analyses confirmed the potential of the ZrB_2–SiC composite to endure re-entry conditions with temperature approaching 2000 °C, thanks to the formation of a steady-state external multiphase oxide scale. Numerical calculations, which simulated the chemical non-equilibrium flow around the ceramic model, matched well the experimental results only assuming a very low catalytic surface behavior.

Keywords: Structural applications; Thermal properties; ZrB_2; SiC

1. Introduction

Improved interest in ultra-high temperature ceramics (UHTCs) is being animating the scientific community over the past decade.[1–4] This emerging attention is driven by the demand of developing re-usable hot structures as thermal protection systems (TPS) of space vehicles able to re-enter from Low Earth Orbit (LEO) at relatively high speed (order of 8 km/s). In contrast to traditional blunt capsules or Shuttle-type vehicles, characterised by poor gliding capabilities and complex TPS, the future use of UHTCs opens new prospects for the development of space planes with slender fuselage noses and sharp wing leading edges. In fact, sharp geometries imply peak heat fluxes in the order of 1 MW/m^2 that state-of-art hot structures such as SiC-coated C–C composites are not able to withstand.[1,4,5] The use of UHTCs would also imply lower aerodynamic drag, improved flight performances and crew safety, due to the larger cross range and manoeuvrability along more gentle re-entry trajectories.[3,6,7]

IV^A group transition metal diborides such as ZrB_2 and HfB_2 have been indicated as promising candidate materials for use in these aerospace applications, primarily for melting temperatures greater than 3200 °C. Other favorable characteristics include high elastic modulus, high thermal conductivity, retained strength at elevated temperature, relatively good thermal shock resistance and modest thermal expansion.[8]

However, pure metal diborides do not fully possess oxidation resistance necessary for surviving reliably the oxidising environment typical of hypersonic re-entry into the Earth atmosphere. Expose HfB_2 to air at elevated temperatures, for instance, leads to form HfO_2 and liquid B_2O_3: above 1600 °C, due to the disruption of the HfO_2 scale when B_2O_3 starts boiling very actively,[9] HfB_2 substantially deteriorates. A special family of diborides-based composites have demonstrated to overcome this limitation, thanks to the incorporation of SiC which improves mechanical properties[10,11] and resistance to oxidation.[1,3,5,9]

From a technological point of view, the effective densification of ZrB_2, due to strong covalent bondings and low self-diffusion coefficients, typically requires sintering temperatures above 2000 °C and applied pressures in atmosphere-controlled furnaces.[12] Instead, several studies demonstrated that SiC added to ZrB_2 enhanced sinter ability and mechanical properties,[10,11]

* Corresponding author. Tel.: +39 0546 699758; fax: +39 0546 46381.
E-mail address: fmonte@istec.cnr.it (F. Monteverde).

0955-2219/$ – see front matter © 2007 Elsevier Ltd. All rights reserved.
doi:10.1016/j.jeurceramsoc.2007.02.201

in addition to the resistance to oxidation[1,13–15] of the diboride alone. For ZrB_2 oxidised in air at elevated temperatures, ZrO_2 and liquid B_2O_3 are formed.[14] Below 1200 °C, molten B_2O_3 glass is basically retained in the porous ZrO_2 structure due to high wettability and considerable surface tension. However, appreciable volatilisation of B_2O_3 starts taking place above 1200 °C,[16] leading to the formation of scarcely protective porous ZrO_2 scale. The addition of SiC to ZrB_2 (for temperatures above 1200 °C) significantly reduces the oxidation rates, thanks to the stability, at much higher temperatures than for the pure diboride, of a protective silica-based glassy layer covering the surfaces exposed to air. Passive-to-active transition of the SiC oxidation has been also observed, resulting in regions beneath the oxide scales formed upon the ZrB_2–SiC base ceramic partially depleted of SiC.[10,14,17]

How UHTCs behave when exposed to convective flows with significant concentrations of atomic oxygen (as is the case of shock waves in hypersonic flows) is a central question that has not received much attention to date. Indeed, a very few number of (expensive) large-scale arc-jet facilities are available for testing UHTCs (and other materials) in hypersonic flows with specific total enthalpies in the order of 10–20 MJ/kg. Thus, the majority of the oxidation studies on UHTCs employed conventional air-furnaces, which ultimately fail to expose materials to significant levels of atomic oxygen.

In this study, microstructure modifications of ZrB_2–SiC composite subjected to arc-jet testing were investigated and discussed. Fluid dynamic numerical calculations were carried out to correlate and explain the experimental results.

2. Experimental

2.1. Material processing

A ZrB_2–SiC ceramic was prepared from commercially available powders of ZrB_2 (grade B, H.C. Starck, Germany) and SiC (BF12, H.C. Starck, Germany). The powder mixture of ZrB_2 + 15 vol.% SiC was ball-milled in ethanol for 1 day using hard milling media, dried with a rotating evaporator, and sieved through a mesh screen with 250 μm openings to minimize agglomeration. The powder blend was then uniaxially hot-pressed in an inductively excited BN-lined graphite die, heating up to 1820 °C (about 20 °C/min average heating rate and 15 min isothermal stage at 1820 °C). The temperature was measured by means of an optical pyrometer focused on the graphite die.

Bulk density and theoretical density were evaluated using the Archimedes' method (water as immersing medium) and the rule-of-mixture, respectively. The relative density was calculated dividing the bulk density by the theoretical density. The phase composition analysis was carried out with a scanning electron microscope (SEM, mod. S360, Leica Cambridge, UK) combined with an energy dispersive X-ray microanalyser (EDS, mod. INCA Energy 300, Oxford Instruments, UK). Polished sections of the as-sintered material were prepared with successively finer diamond-based abrasives ranging from 50 to 0.25 μm.

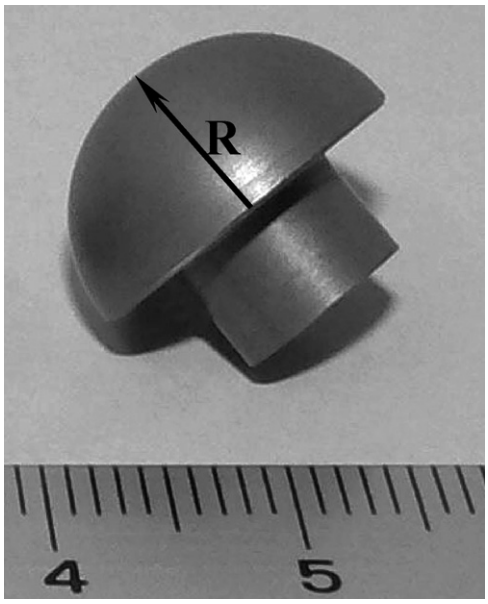

Fig. 1. Hemispheric ZrB_2–SiC model used for arc-jet testing, curvature radius R = 7.5 mm.

Thermal diffusivity (D_{TH}) was measured through the laser flash method (mod. LFA-427, NETZSCH Gerätebau GmbH, Germany), while heat capacity (C_P) using a modulated differential scanning calorimetry (mod. MDSC, TA Instruments, USA). Thermal conductivity (K_{TH}) was estimated through the expression $K_{TH} = D_{TH} C_P \rho$, ρ is the bulk density.

2.2. Plasma torch testing

ZrB_2–SiC models with a hemispheric shape (Fig. 1) were machined through diamond-loaded tools, and then exposed to sustained enthalpy flows using the arc-jet facility available at the University of Naples. The facility is equipped with a 80 kW plasma torch that operates in inert gas (He, N_2, Ar and their mixtures) at mass flow rates up to 5 g/s. Infrared and optical windows in the test chamber allow visual inspection and diagnostic analyses. An automatic control system monitors the main parameters of the apparatus (voltage and current of the arc heater, water cooling temperature, mass flow rate).

In particular, the specific total enthalpy (H) was evaluated through an energy balance between the energy supplied to the gas by the arc heater and the energy transferred to the cooling system (measured by the water temperature jump between inlet and outlet). The output data, processed via a dedicated software, allow not only the evaluation of the surface temperature profile versus exposure time of the model, but also some numerical–experimental correlations.

Due to the extremely high thermal loading upon the ceramic models, surface chemical reactions like oxidation can be responsible for changes in the material's emissivity. To overcome this problem, the experiments were carried out with a radiation ratio pyrometer (Infratherm ISQ5, Impac Electronic Gmbh, Germany) which operates both in two colour and in the single colour function. In the two colour mode the instrument makes use of the ratio of two spectral radiances, measured at different

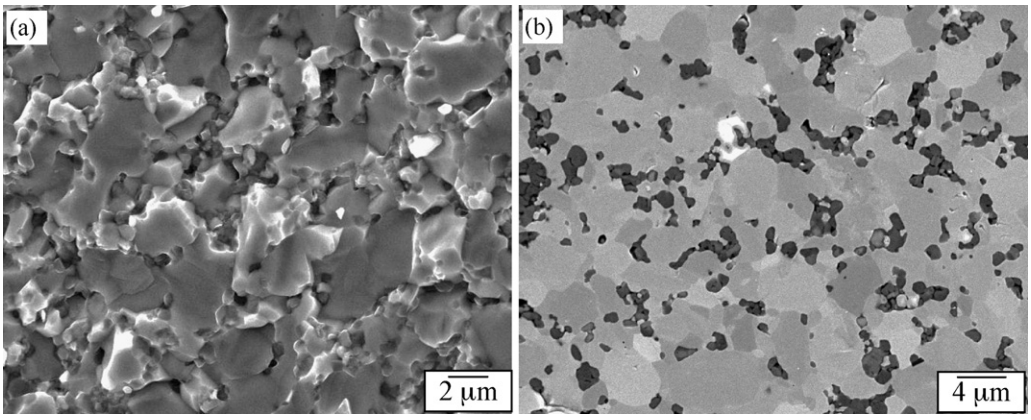

Fig. 2. Fracture (a) and polished surface (b) of ZrB_2–SiC, SEM micrographs: round dark features are SiC (b).

wavelengths (0.9–1.05 μm), to evaluate the true temperature. This overcomes the problem of the emissivity knowledge since it is supposed to be the same at both wavelengths. Once the temperature had been measured with the ratio pyrometer, its value was input to evaluate the spectral emissivity using the single colour function ($\lambda = 0.9$ μm). In combination with the pyrometer, an infrared thermo-camera (Thermacam SC 3000, FLIR Systems, USA) was used to measure the surface temperature distributions and the spectral emissivity in the long wave range of the thermograph ($\lambda = 9$ μm). The ceramic models exposed to the hot stream were further analysed by SEM-EDS on surface and after cross-sectioning. A thin carbon coating was deposited on the analysed surfaces to prevent charging effects.

3. Numerical simulation of the plasma torch flow

To assess if the environment generated by the plasma torch at atmospheric pressure conditions was able to reproduce heat fluxes, temperatures and reactive environments typical of atmospheric re-entry, a systematic numerical analysis has been carried out. The computations have been carried out solving the full Navier–Stokes equations for a turbulent multi-reacting gas mixture with five chemical species (O, O_2, NO, N, N_2) in chemical non-equilibrium. Each species of the mixture was assumed to behave as a thermally perfect gas, where translational-rotational and vibrational-electronic degrees of freedom were characterised by different temperatures. Vibrational-translational energy exchanges have been modeled according to the Landau–Teller model, while the vibrational relaxation time was derived from the Millikan–White formula, with Park correction for high temperatures.[18] Chemical and vibrational non-equilibrium is taken into account using the Park model.[19–21] The fluid-dynamics equations have been numerically solved in the computational domain (plasma torch and test chamber). Convective fluxes were computed according to Roe's Flux Difference Splitting scheme. Integration of the equations was performed implicit in time, until steady state was achieved, solving the linearised system of equation by the multigrid technique.

4. Results and discussion

4.1. Base microstructure

The bulk density of the sintered ZrB_2–SiC pellets was 5.6 ± 0.02 g/cm^3, that corresponds to a relative density higher than 99%. The example of a fracture surface in Fig. 2a reveals the typical grain structure, with regular ZrB_2 grains of about 2 μm average size. The polished section examined by SEM (Fig. 2b) confirmed that the present composite is fully dense (i.e. no apparent porosity). In addition, the investigation by SEM provided evidence of SiC dispersed intergranularly within the ZrB_2 matrix, sometimes in agglomerates (maximum size 5 μm). Detailed SEM-EDS inspections of the microstructure allowed for highlighting also some secondary reaction products in very limited amounts like zirconia and a glass phase among aggregated SiC particles (Fig. 3). A more extensive description is reported elsewhere.[22]

The thermal conductivity (K_{TH}) varied from 62 to 65 W/m K over the temperature range 30–1200 °C. Higher K_{TH} values from 104 to 76.2 W/m K over the temperature range 30–1200 °C were reported for an UHTC composed of $ZrB_2 + 20$ vol.% SiC.[23]

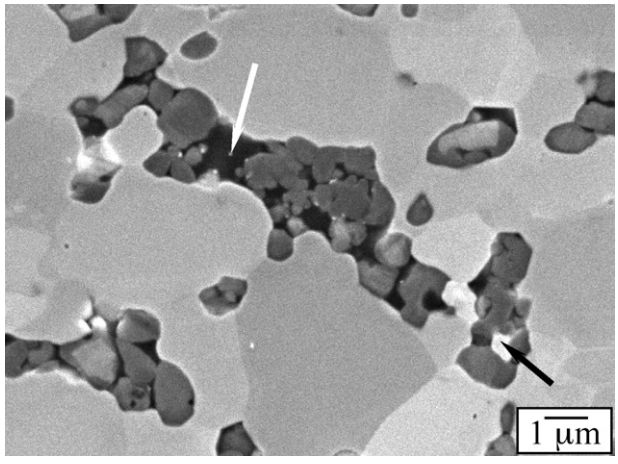

Fig. 3. Polished section of ZrB_2–SiC, SEM micrograph: glass phase (white arrow) and zirconia (black arrow) are marked.

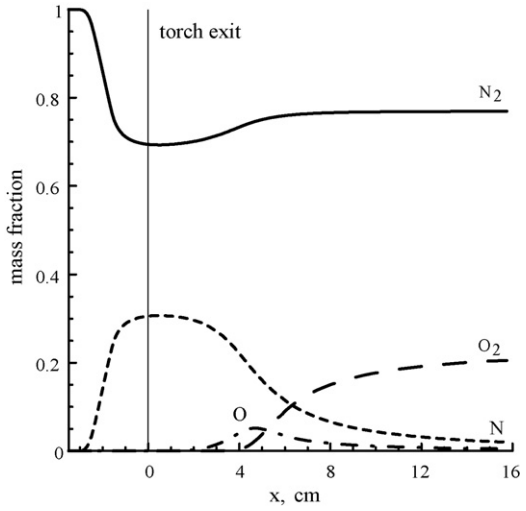

Fig. 4. Computed mass fractions of the different species along the torch axis (x).

A variation in K_{TH} was likewise observed in the HfB_2–SiC system.[3]

4.2. Plasma flow characterisation

The numerical simulations herein presented refer to a Nitrogen plasma jet with mass flow rate of 1 g/s, for a power transferred to the fluid of 15 kW: mass fraction profiles of different species along the symmetry axis of the torch (Fig. 4), and specific total enthalpy along the symmetry axis of the exhaust jet (Fig. 5) are shown. At the exit of the torch the partially dissociated Nitrogen expands through a nozzle (5 mm in diameter), comes into contact with the surrounding air at ambient conditions, so that oxygen in the atmosphere dissociates and a reacting mixture composed by O_2, N_2, NO, O, N is formed (Fig. 4). The specific total enthalpy decreases rapidly along the torch axis (Fig. 5). Changing the distance between the torch exit and the specimen, different conditions can be established. In

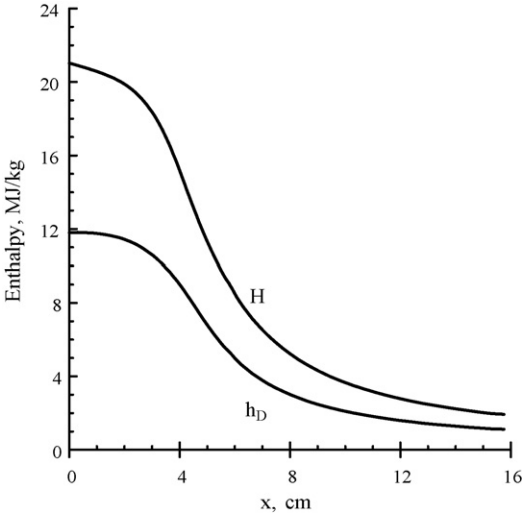

Fig. 5. Computed specific total enthalpy H and specific chemical enthalpy h_d along the torch axis x, $x = 0$ the torch outlet.

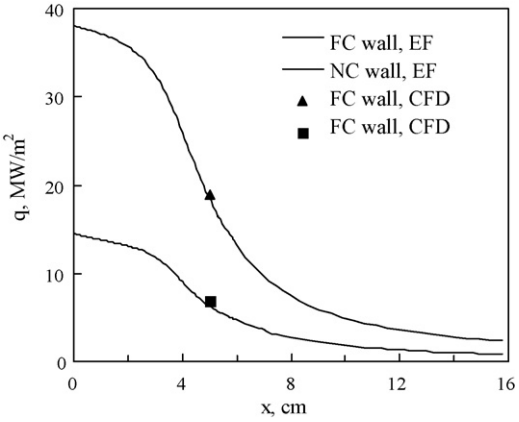

Fig. 6. Stagnation point heat flux (q) computed at different distances from the exit torch (x). The continuous lines correspond to the engineering formulas (EF) for the different assumptions of fully catalytic (FC) and non catalytic (NC) wall. The two points are evaluated with computation fluid dynamics (CFD).

particular, the range of interest is between 4 and 12 cm, with a corresponding decrease of the specific total enthalpy from about 18 to 3 MJ/kg. Fig. 5 also shows the contribution of the specific chemical enthalpy (h_d) to the specific total enthalpy due to the dissociated chemical species. The numerical results have been interpolated to show that the here reported semi-empirical formulas found for the stagnation point heat flux (q) at hypersonic conditions[24]

$$\dot{q}_{FC} = 2.75 \times 10^{-5} \sqrt{\frac{p}{R}} (H_0 - h_w)^{1.17}, \qquad \dot{q}_{NC} = 2.75 \times 10^{-5} \sqrt{\frac{p}{R}} (H_0 - h_d - h_w)^{1.17} \tag{1}$$

are still valid in these conditions, where the NC and FC subscripts refer to a non catalytic wall and to a fully catalytic wall, respectively, H_0 is the specific total enthalpy at the exit of the torch, h_d is the chemical enthalpy stored in the atomic species; h_w is the wall enthalpy, R the gas constant and p the stagnation point pressure. In Fig. 6 the stagnation point heat fluxes evaluated with the semi-empirical formulas are compared to the computational fluid dynamics (CFD) results and a good agreement is found.

4.3. Arc-jet testing

The present ZrB_2–SiC composite was subjected to arc-jet testing which, as verified in Section 4.2, enabled a ground simulation of conditions expected during an atmospheric re-entry. In particular, the hemispheric models (Fig. 1) were exposed to a reactive gas mixture with an average total enthalpy in the order of 10–20 MJ/kg. Fig. 7a shows the temperature profiles of the model's surface during two arc-jet tests. During the test numbered 1 in Fig. 7a, the average specific total enthalpy was 17.3 MJ/kg during the first 60 s; the arc current was then increased and the specific total enthalpy reached a value of 19.7 MJ/kg and was maintained for approximately 270 s. In the test numbered 2 in Fig. 7a, a similar procedure was applied and the specific total enthalpy was 14.8 MJ/kg during the first 60 s and 16.6 MJ/kg for about 1 min. The corresponding values of

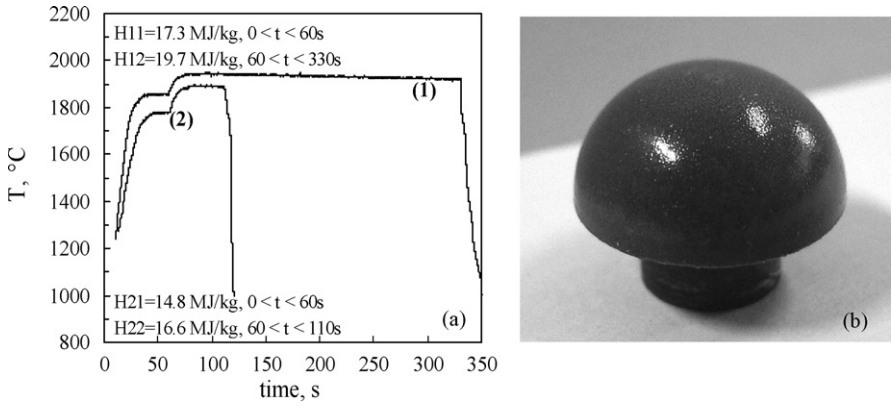

Fig. 7. Temperature (T) profiles vs. time during arc-jet testing of the ZrB_2–SiC model (a), and its post-test appearance (b); specific total enthalpies during test_1 (H_{11} and H_{12}) and test_2 (H_{21} and H_{22}) are indicated.

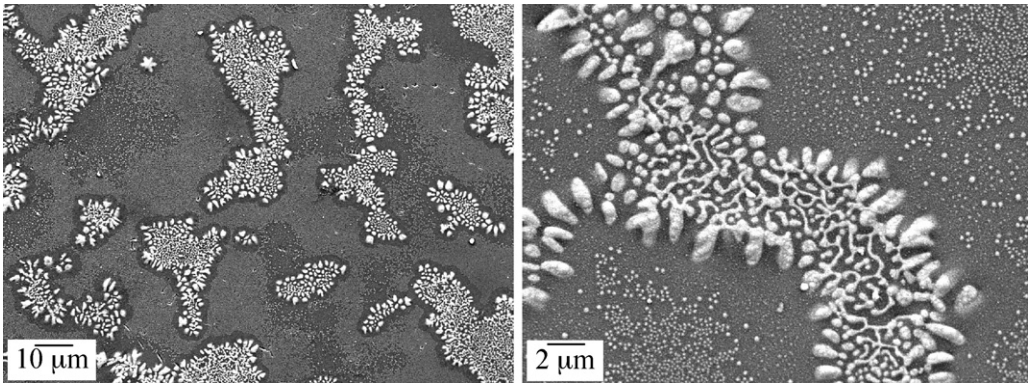

Fig. 8. Surface of the ZrB_2–SiC model after arc-jet testing (refer to the curve_1 in Fig. 7a), SEM micrographs.

the stagnation point heat fluxes, computed by numerical simulations, are in the order of 8–10 MW/m^2. In both cases, a value of about 0.9 was found for the emissivity at the highest temperatures. Just for comparison, arc-jet tests performed on ZrB_2–SiC and HfB_2–SiC materials elsewhere described[3,14] involved stagnation point heat fluxes in the order of 3.5–4 MW/m^2.

With reference to the test numbered 1 in Fig. 7a, the surface temperature of the (hemispheric) model rose during exposure up to 1850 °C within about 1 min. Increasing the specific total enthalpy up to about 20 MJ/kg, the surface temperature rapidly reached a value of about 1930 °C, followed by a slow decay to 1910 °C for the remaining duration of the test (i.e. 5 min). After exposure, the specimen appeared slightly glazed, but maintained an apparent integrity: a post-test picture of the model is displayed in Fig. 7b. Analyses by SEM-EDS of the exposed surface revealed a coherent and smooth silica glass coating decorated with partly aggregated zirconia crystals of various size and shape (Fig. 8). Silicon and oxygen apart, neither zirconium nor boron were detected in the (outermost part of the) external glass.

To have a more detailed insight into the microstructure evolution upon the model's surface during exposure, a specimen was tested at very similar conditions (specific total enthalpy 16.6 MJ/kg and total duration of about 2 min, see curve 2 in Fig. 7b). Though the visual appearance does not bring on significant differences compared to the test numbered 1 (Fig. 7a) early described, the model's surface after this exposure revealed clustered craters at the top of a glass coating (Fig. 9). The typical aggregations of zirconia crystals previously emphasised in Fig. 8 were not observed.

The cross-sectioning and polishing of the models after arc-jet testing provided insight into microstructure details of great interest. The elemental mapping by SEM-EDS throughout the oxidised cross-section revealed the formation of a multiphase layered structure (Figs. 10 and 11). The outermost layer, a few microns thick, consists of silica, and adheres to an oxide sub-scale, 20 μm thick. The lastly cited scale includes zirconia

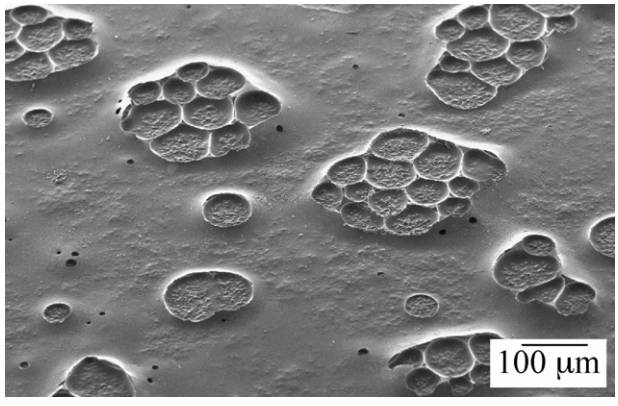

Fig. 9. Surface of the ZrB_2–SiC model after arc-jet testing (refer to the curve_2 in Fig. 7a), SEM micrograph.

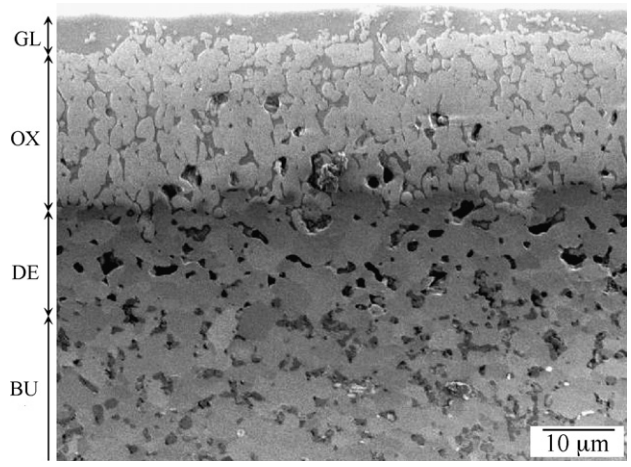

Fig. 10. Cross-section of the ZrB_2–SiC model after arc-jet testing (refer to the curve_1 in Fig. 7a), SEM micrograph; the oxide sub-scale (OX) underlying the external glass layer (GL), and the SiC-depleted region (DE) close to the virgin bulk (BU) are shown.

crystals embedded within a glass whose composition does not differ significantly from that located on the surface. Underneath, a layer partly depleted of SiC (10 μm thick) has formed, and underlines the un-altered ZrB_2–SiC matrix. The creation of such an inner porosity most likely was caused by the active oxidation of SiC, which represents a well-known phenomenon in SiC and SiC-containing materials.[25–26] The interface between the fully oxidised scale and that partially depleted of SiC appears sharp, i.e. any transitional regions have formed. The external glass coverage apart, analogous multilayered structures were observed in MB_2-SiC models subjected to arc-jet testing.[3,14,27]

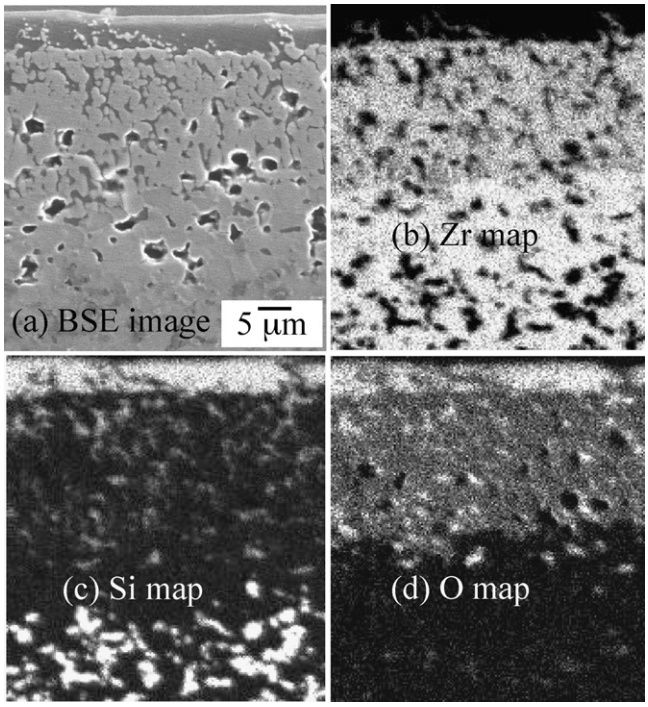

Fig. 11. Cross-section of the ZrB_2–SiC model after arc-jet testing (refer to the curve_1 in Fig. 7a, SEM micrograph by back-scattered electrons) and associated elemental maps by SEM-EDS.

The SEM-EDS analysis of the cross-sectioned specimen associated to curve 2 in Fig. 7a (duration of about 2 min) presented very similar details. However, different from the ZrB_2–SiC model arc-jet tested according to curve 1 in Fig. 7a, the occurrence of a pitted surface was linked to reactions involving the evolution of gaseous by-products. In fact, during the initial exposure to such harsh convectively heating conditions, SiO, B_2O_3 and other highly volatile boron sub-oxides, which tend to evolve outside, most likely coalesced in bubbles inside the external forming glass. Shear forces associated to the hot stream facilitated the bursting of bubbles and, for prolonged exposure (curve 1 in Fig. 7a), the smoothing of the outermost glassy coating. According to the SEM-EDS analytical resolution, silicon and oxygen apart, the characteristic peaks for boron and zirconium, due to the very low intensities, were of uncertain attribution. The postulation of mass loss mechanisms were not correlated to quantitative evaluations of weight changes and size recession of the models.

The arc-jet tests presented in Fig. 7a provided an indication for the potential of this material for sharp leading edge applications: the significance of the microstructure changes after exposure to (simulated) re-entry conditions resulted within acceptable limits. It is the authors opinion that reasons for the configurational stability coupled to the high oxidation resistance of the present UHTC when subjected to heat fluxes typical of a re-entry environment should be inquired into the coherence of the passivating oxide scales covering its surfaces. The multiphase oxide scales of the present UHTC maintain protective capabilities even at extremely high temperatures thanks to the prompt recovery after bubble bursts: in that case, viscosity of the glass as well as its wetting behavior to the underlying oxide scale played a fundamental role. When the model's temperature levelled off at about 1930 °C (test 1 in Fig. 7a), the passivating silica layer which formed from the oxidation of SiC supported the maintenance of a steady state temperature. In addition, the condensation of volatile SiO (and boron sub-oxides) at the base of the oxide sub-scale (Fig. 10) could explain the stability of that microstructure as a quasi steady-state region, volatilising from the outer surface and re-constituting at lower depth. The crystalline zirconia that appears adherent to the formed glass (Figs. 10 and 11) suggests an extremely low solubility between the cited couple of compounds. Due to the preferential evaporation of boron oxides, precipitates of zirconia decorating the outermost glass layer after a relatively long exposure may indicate a change in ZrO_2 solubility for borosilicate glasses versus the pure B_2O_3.

The improved performances of this material under strong heat flux conditions are deemed to arise also from its high thermal conductivity. This requisite allows heat to be conducted from the stagnation points to colder zones, and from there re-radiated away. In this respect, this class of UHTCs differs a typical insulating thermal protection structure which rejects heat almost solely by radiation. In addition, surface emissivities at very high temperatures around 0.9 helped the material maintain steady state surface temperature, levelling off for instance around 1930 °C as in the test early described in Fig. 7a.

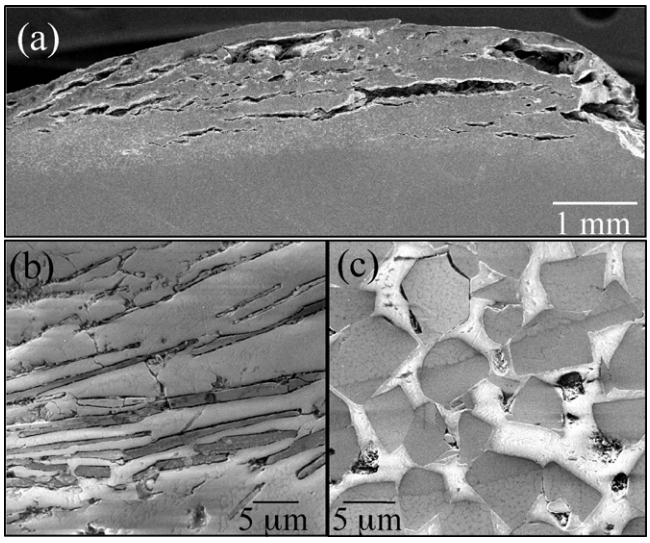

Fig. 12. Cross-section of the ZrB_2–SiC model after arc-jet testing (surface peak temperature 2400 °C): a general view (a) and details of heavily altered zones (b and c) are shown, SEM nicrographs.

Limited applicability is however expected when the multilayer oxide scales stop mitigating the influence of high pressure inner gaseous by-products like SiO, B_2O_3 and CO that find ways to evolve outside disruptively. In this respect, an additional arc-jet test was carried out in the same environment but at extremely high heat fluxes (higher than 10 MW/m^2). The temperature climbed up so rapidly to about 2400 °C within 20 s that the tested model was unable to offer a valuable resistance to the aero-thermal load applied, and a stable configuration was never established. A large activity of volatile products due to the violent jump in temperature occurred in proximity of the hottest zones, leading to micro/macro-spallation of the model surface (Fig. 12a). Due to the multiform variety of the altered regions, a comprehensive description resulted an hardly solvable task. For sake of simplicity, examples of some intriguing features are given in Fig. 12b and c. The extent of the damage in these conditions is to be considered not acceptable for the foreseen demand of reliability and re-usability.

4.4. Role and influence of dissociated oxygen

The present work has been inserted into the experimental effort that has recently begun to address the question if oxidation of SiC-containing metal borides based materials in dissociated oxygen, the primary oxidant in a re-entry environment, proceeds more rapidly than that by molecular oxygen. Preliminary indications seem confirmatory.[4] However, aspects like the characteristics of the oxide scales produced by oxygen atoms, or the passive-to-active oxidation boundaries of SiC remain basically unexplored. Atomic oxygen for instance is reported to accelerate oxidation rates in a variety of metals, ceramics and semiconductors.[4] A series of experiments by Balat et al. showed that the temperature-pressure boundary between passive-to-active oxidation of SiC can be shifted significantly if atomic oxygen is present.[25] Rogers and co-workers, studying the oxidation behavior of UHTCs and their constituents at high temperature, found dramatically enhanced oxidation rates on Si, SiC and Si_3N_4 in dissociated versus molecular oxygen, under the same temperature and pressure.[28]

As the oxide scales development in a oxidising (re-entry) environment is concerned, it actually involves the composite interaction of factors primarily associated with mass transport. In contrast to oxidation studies in conventional high temperature furnaces where the primary oxidant is the molecular oxygen,[10,13–15,17,22] the transport mechanisms governing oxidation under an oxygen atom exposure are not yet clearly identified, even in pure silica scales. In fact, while the diffusion of interstitial molecular oxygen seems confirmed as the dominant oxygen transport process within amorphous silica, what happens when oxygen atoms are the major oxidant agent arriving at the surface does not find a shared explanation yet. Instead, the multilayer oxide scales formed upon oxidation tests in conventional furnaces and in simulated atmospheric re-entry conditions[3,9,14,17,27] show however similarities. In the present case, an heat treatment at 1450 °C of 20 h in flowing air at ambient pressure revealed a rather similar layered configuration.[22] The oxidation of ZrB_2–SiC in air was also analysed using volatility diagrams for ZrB_2 and SiC.[29,30] The diagrams justified, thermodynamically, formation and stability of the outermost silica coating as well as the development of SiC-depleted regions beneath the outer oxide scales. The question whether atmospheric re-entry conditions characterised by equivalent temperatures and dwell times, induce varying thickness of the separate oxide scales is matter of future work.

Other open topics connected to the consequences of the oxidation in presence of a reactive hot stream containing dissociated oxygen are currently receiving much attention. Does dissociated oxygen recombine at the surface or within the silica-based glass? Does it then diffuse inward in molecular form? In this respect, the experimental temperature–time profiles (Fig. 7) matched adequately the calculated heat flux distribution only assuming a non catalytic behavior with reference to the oxygen recombination (see specific comments in Section 4.5). It should be pointed out that the present tests have been carried out at atmospheric pressure conditions. Experimental and theoretical works on the catalytic activity of silica-based materials under simulated re-entry conditions[31,32] have shown that the catalytic atomic recombination coefficients, for a constant temperature, are decreasing functions of the pressure. Therefore the catalytic properties of the material, in respect to the recombination of oxygen atoms, may be larger at lower pressures, as found for instance in arc-jet experiments with ZrB_2/SiC and HfB_2/SiC ceramic materials.[2]

It should also be emphasised that the co-existence of crystalline (i.e. zirconia) and amorphous (i.e. silica) phases constituting the multiphase oxide scales makes the establishment of the rate-limiting transport extremely difficult. In contrast to the amorphous silica behavior, the monoclinic crystal structure of zirconia for instance favors oxygen incorporation and diffusion in ionic rather than in molecular form. This suggest that the dissociated oxygen in the reactive gas mixture enhances oxidation since its incorporation into the zirconia scale would not require an endothermic dissociation reaction. To conclude, although the

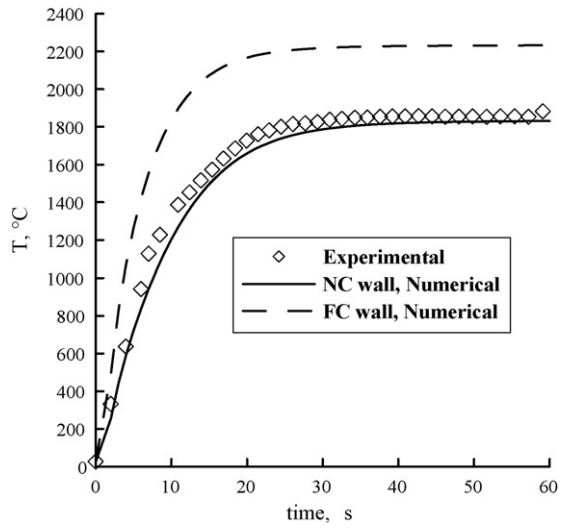

Fig. 13. Experimental results and numerical solutions corresponding to the different assumption of fully catalytic (FC) and non catalytic (NC) wall, 14.8 MJ/kg of specific total enthalpy.

ZrB_2–SiC composite already displayed encouraging technical merits to be a valuable candidate in aerospace applications, many facets of the resistance to oxidation in re-entry conditions need further confirmations in order to extend this technological challenge for repeated safe uses.

4.5. Experimental-numerical correlation of aerothermal heating

Numerical computations have been carried out, using the model described in Section 3, under two different assumptions about the catalytic properties of the specimen surface with reference to recombination of atomic oxygen. The simulations refer to the plasma torch test characterised by a specific total enthalpy of 14.8 MJ/kg (whose results are shown in curve 2 of Fig. 7a) assuming the two extreme situations of a non catalytic wall and a fully catalytic wall.[33] Based on the computed heat flux distributions, a thermal analysis has been carried out in both cases to evaluate the corresponding time profiles of the temperature. Fig. 13 shows the results computed under the two assumptions of fully catalytic and non catalytic wall, and the experimental profile obtained with the pyrometer. Fig. 13 shows that the experimental results match quite well the numerical ones corresponding to the non catalytic wall condition. This points out that the material herein tested exhibits, at very high temperatures, a non catalytic behavior. This behavior can be explained by the formation of a silica surface thin layer (Figs. 9–11) which is known to possess very low catalytic recombination behavior.[33,34] The presence of such a surface layer also justifies the high values of the surface emissivity, according to the literature data.[35]

5. Summary and future work

An ultra-high temperature dense ZrB_2–SiC ceramic was produced by hot-pressing. Hemispheric ZrB_2–SiC models (curvature radius 7.5 mm) were exposed to ground simulated atmospheric re-entry conditions using arc-jet testing, with an average specific total enthalpy (H) in the order of 10–20 MJ/kg. The model's surface reached a peak value of 1930 °C within 1 min for H approaching 20 MJ/kg. Elemental mapping by SEM-EDS of the cross-section after exposure showed a rather compact scale of zirconia (20 μm thick) underlying a thin silica-based smooth coating. A partially SiC-depleted region underneath the zirconia scale, a few microns thick, was also seen. Formation of a steady-state external multiphase oxide scales and high thermal conductivity were indicated and therefore discussed as the favorable factors which provided a considerable potential for this material in sharp leading edge applications. Numerical calculations, which simulated the chemical non-equilibrium flow around the hemispheric model correlated well with the experimental results only assuming a very low catalytic surface behavior (with reference to the oxygen recombination). Additional work needs to address the key question if this class of materials oxidises in dissociated oxygen more rapidly than in air-atmosphere. Moreover, correlate dimensional stability-oxidation rates-active oxidation of SiC is of priority relevance.

Acknowledgements

The authors would like to thank D. Dalle Fabbriche (ISTEC) and P. Loquace (DIAS) for their technical assistance.

References

1. Upadhya, K., Yang, J.-M. and Hoffman, W., Materials for ultrahigh temperature structural applications. *Am. Ceram. Soc. Bull.*, 1997, **76**(12), 51–56.
2. Marschall, J., Chamberlain, A., Crunkleton, D. and Rogers, B., Catalytic atom recombination on ZrB_2/SiC and HfB_2/SiC ultrahigh-temperature ceramic composites. *J. Spacecraft Rockets*, 2004, **41**(4), 576–581.
3. Gasch, M., Ellerby, D., Irby, E., Beckman, S., Gusman, M. and Johnson, S., Processing, properties and arc-jet oxidation of hafnium diboride/silicon carbide ultra high temperature ceramics. *J. Mater. Sci.*, 2004, **39**, 5925–5937.
4. Bongiorno, A., Forst, C. J., Kalia, R. K., Li, J., Marschall, J., Nakano, A. *et al.*, A perspective on modeling materials in extreme environments: oxidation of ultrahigh-temperature ceramics. *MRS Bull.*, 2006, **31**, 410–418.
5. Richet, N., Lespade, P., Goursat, P. and Laborde, E., Oxidation resistance of HfB_2–SiC coatings for protection of carbon fiber based composites. *Key Eng. Mater.*, 2004, **264–268**(TTP), 1047–1050.
6. Janowski, R., Tauche, M., Scheper, M., Monti, R. and Savino, R., Space plane: a new way for atmospheric reentry. In *Proceedings of the 1st International ARA Days, Atmospheric Reentry Systems, Missions and Vehicles. Session 15-System Design*, 2006.
7. Monti, R., De Stefano, M. and Savino, R., Thermal shielding of a reentry vehicle by ultra high temperature ceramic materials. *J. Thermophys. Heat Transfer*, 2006, **20**(3), 500–506.
8. Cutler, R. A., Engineering properties of borides. In *Ceramics and Glasses, Engineered Materials Handbook*, *Vol 4*, ed. S. J. Schneider. ASM International, Materials Park, OH, 1992.
9. Metcalfe, A. G., Elsner, N. B., Allen, D. T., Wuchina, E., Opeka, M. and Opila, E., Oxidation of hafnium diboride. In *High Temperature Corrosion and Materials Chemistry: Per Kofstad Memorial Symposium, Electrochemical Society Proceedings, Vol 99-38*, 1999, pp. 489–501.
10. Monteverde, F., Beneficial effects of an ultra-fine α-SiC incorporation on the sinterability and mechanical properties of ZrB_2. *Appl. Phys. A*, 2006, **82**, 329–337.
11. Chamberlain, A. L., Fahrenholtz, W. G. and Hilmas, G. E., High-strength zirconium diboride-based ceramics. *J. Am. Ceram. Soc.*, 2004, **87**(6), 1170–1172.

12. Pastor, H., Metallic borides: preparation of solid borides—sintering method and properties of solid bodies. In *Boron and Refractory Borides*, ed. V. I. Matkovich. Springer Verlag, New York, 1977.
13. Tripp, W., Davis, H. and Graham, H., Effect of an SiC addition on the oxidation of ZrB_2. *Am. Ceram. Soc. Bull.*, 1973, **52**(8), 612–616.
14. Chamberlain, A., Fahrenholtz, W., Hilmas, G. and Ellerby, D., Oxidation of ZrB_2–SiC ceramics under atmospheric and re-entry conditions. *Refract. Appl. Trans.*, 2005, **1**(2), 1–8.
15. Monteverde, F. and Bellosi, A., Oxidation of ZrB_2 based ceramics in air. *J. Electrochem. Soc.*, 2003, **150**(11), B552L B559.
16. Fahrenholtz, W., The ZrB_2 volatility diagram. *J. Am. Ceram. Soc.*, 2005, **88**(12), 3509–3512.
17. Rezaie, A., Fahrenholtz, W. and Hilmas, G., Oxidation of zirconium diboride–silicon carbide at 1500 °C at low partial pressure of oxygen. *J. Am. Ceram. Soc.*, 2006, **89**(10), 3240–3245.
18. Park, C., *Nonequilibrium Hypersonic Aerothermodynamics*. John Wiley & Sons, 1990.
19. Park, C., Review of chemical-kinetic problems of future NASA missions. I. Earth Entries. *J. Thermophys. Heat Transfer*, 1993, **7**(3), 385–398.
20. Park, C., Howe, J. T., Jaffe, R. L. and Chandler, G. V., Review of chemical-kinetic problems of future NASA missions. II. Mars entries. *J. Thermophys. Heat Transfer*, 1994, **8**(1), 9–23.
21. Park, C., Jaffe, R. L. and Partridge, H., Chemical-kinetic parameters of hyperbolic earth entry. *J. Thermophys. Heat Transfer*, 2001, **15**(1), 76–90.
22. Monteverde, F. and Scatteia, L., Resistance to thermal shock resistance and to oxidation of metal diborides-SiC ceramics designed for aerospace application. *J. Am. Ceram. Soc.*, 2007, **90**, 1130–1138.
23. Thomas, D., *Design and analysis of UHTC leading edge attachment*. NASA/CR – 2002-211505, 2002.
24. De Filippis, F., Savino, R. and Martucci, A., Numerical-experimental correlation of stagnation point heat flux in high enthalpy hypersonic wind tunnel. In *Proceedings of the 13th AIAA/CIRA International Space Plane and Hypersonic Systems and Technologies Conference*, 2005.
25. Balat, M. and Berjoan, R., Oxidation of sintered silicon carbide under microwave-induced CO_2 plasma at high temperature: active–passive transition. *Appl. Surf. Sci.*, 2000, **161**, 434–442.
26. Hald, H., Operational limits for re-usable space transporation systems due to physical boundaries of C/SiC materials. *Aerospace Sci. Technol.*, 2003, **7**, 551–559.
27. Bull, D., Rasky, D. J. and Karika, J. C., Stability characterization of diboride composites under high velocity atmospheric flight conditions. In *Proceedings of the 24th International SAMPE Technical Conference*, 2002, pp. T1092–T1116.
28. Rogers, B., Song, Z., Marschall, J., Queraltò, N. and Zorman, C. A., *High Temperature Corrosion and Materials Chemistry*, *Vol 268*, ed. V. E. Opila. The Electrochemical Society, Pennington, 2004.
29. Fahrenholtz, W., Thermodynamic analysis of ZrB_2–SiC oxidation: formation of a SiC-depleted region. *J. Am. Ceram. Soc.*, 2007, **90**(1), 143–148.
30. Wang, C. R., Yang, J.-M. and Hoffman, W., Thermal stability of refractory carbide/boride composites. *Mater. Chem. Phys.*, 2002, **74**, 272.
31. Kolesnikov, A. F., Gordeev, A. N., Vasil'evskii, S. A. and Verant, J. L., Predicting catalytic properties of SiC material for the Pre-X vehicle reentry conditions. In *Proceedings of the First European Conference for Aerospace Sciences (EUCASS)*, 2005.
32. Kolesnikov, A. F., Yakushin, M. I., Pershin, I. S., Vasil'evskii, S. A., Chaot, O., Vancrayenest, B. *et al.*, Comparative study of surface catalyticity under subsonic air test conditions. In *Proceedings of the 4th Europ. Symp. Aerothermodynamics for Space Applications*, 2001, pp. 481–486, ESA SP-487.
33. Greaves, J. C. and Linnett, J. W., Recombination of atoms at surfaces. Part 5. Oxygen atoms at oxide surfaces. *Trans. Faraday Soc.*, 1959, **55**, 1346.
34. Dickens, P. G. and Sutcliffe, M. B., Recombination of oxygen atoms on oxide surfaces. Part 1. Activation energies of recombination. *Trans. Faraday Soc.*, 1964, **60**, 1272.
35. Wolfe, W. L. and Zissis, G. J., *The Infrared Handbook*. Environmental Research Institute of Michigan, 1978.